J. Biochem. **138**, 343–353 (2005)
doi:10.1093/jb/mvi133

Stabilization Mechanism of the Tryptophan Synthase α-Subunit from *Thermus thermophilus* HB8: X-Ray Crystallographic Analysis and Calorimetry

Yukuhiko Asada[1], Masahide Sawano[1], Kyoko Ogasahara[2], Junji Nakamura[3], Motonori Ota[4], Chizu Kuroishi[1], Mitsuaki Sugahara[1], Katsuhide Yutani[1] and Naoki Kunishima[1,*]

[1]Advanced Protein Crystallography Research Group, RIKEN Harima Institute at SPring-8, 1-1-1 Kouto, Mikazuki-cho, Sayo-gun, Hyogo 679-5148; [2]Institute for Protein Research, Osaka University, 3-2 Yamadaoka, Suita, Osaka 565-0871; [3]Nihon SiberHegner KK, Tokyo Ryutsu Center, BE4-1, 6-1-1 Heiwajima, Oota, Tokyo 143-6591; and [4]Global Scientific Information and Computing Center, Tokyo Institute of Technology, 2-12-1 Ookayama, Meguroku, Tokyo 152-8550

Received April 5, 2005; accepted June 27, 2005

In order to elucidate the thermo-stabilization mechanism of the tryptophan synthase α-subunit from the extreme thermophile *Thermus thermophilus* HB8 (*Tt*-α-subunit), its crystal structure was determined and its stability was examined using DSC. The results were compared to those of other orthologs from mesophilic and hyperthermophilic organisms. The denaturation temperature of the *Tt*-α-subunit was higher than that of the α-subunit from *S. typhimurium* (*St*-α-subunit) but lower than that of the α-subunit from *P. furiosus* (*Pf*-α-subunit). Specific denaturation enthalpy and specific denaturation heat capacity values of the *Tt*-α-subunit were the lowest among the three proteins, suggesting that entropy effects are responsible for the stabilization of the *Tt*-α-subunit. Based on a structural comparison with the *St*-α-subunit, two deletions in loop regions, an increase in the number of ion pairs and a decrease in cavity volume seem to be responsible for the stabilization of the *Tt*-α-subunit. The results of structural comparison suggest that the native structure of the *Tt*-α-subunit is better adapted to an ideally stable structure than that of the *St*-α-subunit, but worse than that of the *Pf*-α-subunit. The results of calorimetry suggest that the residual structure of the *Tt*-α-subunit in the denatured state contributes to the stabilization.

Key words: DSC, protein stability, protein structure, thermophile, *Thermus thermophilus*, tryptophan synthase α-subunit, X-ray analysis.

Abbreviations: *Tt*-α-subunit, tryptophan synthase α subunit from *Thermus thermophilus* HB8; *Pf*-α-subunit, tryptophan synthase α subunit from *Pyrococcus furiosus*; *St*-α-subunit, tryptophan synthase α subunit from *Salmonella typhimurium*; *St*-$\alpha_2\beta_2$ complex, tryptophan synthase $\alpha_2\beta_2$ complex from *Salmonella typhimurium*; DSC, differential scanning calorimetry; *ASA*, accessible surface area; rmsd, root mean square deviation.

Proteins from thermophiles are suitable to investigate the stabilization mechanism of proteins because they are remarkably stable compared with their orthlogs from mesophiles. To date, the crystal structures of many proteins from various thermophiles have been determined and compared in order to elucidate the mechanism of the extremely high stability of these proteins (*1*). Many stabilization factors responsible for the high stability have been proposed based on structural features such as (i) a decrease in solvent-exposed surface area (*2*), (ii) an increase in packing density (*3*, *4*), (iii) an increase in core hydrophobicity (*5*, *6*), (iv) a decrease in the length of surface loops (*4*), (v) an increase in the number of hydrogen bonds (*7*), and (vi) a significant increase in the number of ion pairs (*8–16*). However, the molecular origin of the high stability of thermophile proteins remains to be elucidated. To address these questions, the thermodynamic properties of denaturation in solution should be examined, and the stabilization mechanism should be elucidated on the basis of their three-dimensional structures.

Prokaryotic tryptophan synthase [EC 4.2.1.20], which catalyzes the last processes in the biosynthesis of tryptophan, is a multimeric $\alpha_2\beta_2$ complex composed of nonidentical α and β subunits. This $\alpha_2\beta_2$ complex has an αββα arrangement (*17*) and can be isolated as α monomers and β_2 dimers. The α and β_2 subunits catalyze different reactions. The crystal structures of the tryptophan synthase $\alpha_2\beta_2$ complex from *Salmonella typhimurium* (*17*) and that of the α-subunit from *Pyrococcus furiosus* (*Pf*-α-subunit) (*16*) have been determined. On the basis of structural information about the α-subunit from *S. typhimurium* (*St*-α-subunit) and the *Pf*-α-subunit, it has been reported (*16*) that hydrophobic interactions in the protein interior do not contribute to the higher stability of the *Pf*-α-subunit, and that an increase in ion pairs, a decrease in cavity volume, and entropic effects due to shortening of the polypeptide chain play important roles in the extremely high stability. Furthermore, calorimetric results have indicated

*To whom correspondence should be addressed. Tel: +81-791-58-2937, Fax: +81-791-58-2917, E-mail: kunishima@spring8.or.jp

experimentally that the *Pf*-α-subunit has extremely high thermostability, and that its higher stability is caused by entropic effects (*16*).

It will be interesting to examine whether tryptophan synthase α-subunits from other thermophiles are also stabilized by entropic effects, in order to elucidate the thermostabilization mechanism of thermophile proteins. Therefore, we chose the tryptophan synthase α-subunit from the extreme thermophile *Thermus thermophilus* HB8 (*Tt*-α-subunit), whose optimum growth temperature of 75°C is lower than the 95°C of the hyperthermophile *P. furiosus*. Then, we determined the crystal structure of the *Tt*-α-subunit at 1.34 Å resolution. The stability of the *Tt*-α-subunit was evaluated experimentally using differential scanning calorimetry (DSC). In this paper, we discuss the thermostabilization mechanism of the *Tt*-α-subunit on the basis of the crystal structures and DSC data of the α-subunit orthologs from mesophilic, extreme thermophilic, and hyperthermophilic organisms.

MATERIALS AND METHODS

Protein Expression and Purification—The expression plasmid pET-11a, which carries a gene encoding the *Tt*-α-subunit (residues 1–271) from the *Thermus thermophilus* HB8 genome (*18*), was prepared by the RIKEN Structurome Group. The recombinant plasmid was transformed into *Escherichia coli* BL21 (DE3) cells and grown at 37°C in LB medium containing 50 μg/ml ampicillin for 20 h. The cells were harvested by centrifugation at 4,500 × *g* for 5 min, suspended in 20 mM Tris-HCl, pH 8.0 (buffer A), containing 0.5 M NaCl and 5 mM 2-mercaptoethanol, and disrupted by sonication. The supernatant was heated at 70°C for 13 min. After the heat treatment, cell debris and denatured proteins were removed by centrifugation at 20,000 × *g* for 30 min, and the supernatant solution was used as the crude extract for purification. The crude extract was desalted on a HiPrep 26/10 desalting column (Amersham-Biosciences) and applied onto a SuperQ TOYOPEARL 650 M column (Tosoh) equilibrated with buffer A. Proteins were eluted with a linear gradient of 0–0.3 M NaCl. The fraction containing the *Tt*-α-subunit was desalted with HiPrep 26/10 and subjected to a RESOURCE Q column (Amersham-Biosciences) equilibrated with buffer A. After elution with a linear gradient of 0–0.2 M NaCl, the fraction containing the *Tt*-α-subunit was desalted with HiPrep 26/10 equilibrated with 10 mM phosphate-NaOH, pH 7.0, and applied onto a Bio-Scale CHT-20-I column (BIO-RAD) equilibrated with the same buffer. After the elution with a linear gradient of 10–100 mM phosphate-NaOH, pH 7.0, and replacement of the buffer with buffer A, the fraction containing the *Tt*-α-subunit was subjected to a RESOUCE S6 column (Amersham-Biosciences) equilibrated with 20 mM MES-NaOH, pH 6.0. Proteins were eluted with a linear gradient of 0–200 mM NaCl. The fractions containing the *Tt*-α-subunit were pooled, concentrated by ultrafiltration (Amicon, 5 k cut) and loaded onto a HiLoad 16/60 Superdex 200 pg column (Amersham-Biosciences) equilibrated with buffer A containing 0.2 M NaCl. The purified protein showed a single band on SDS–polyacrylamide gel electrophoresis. The concentration of the protein was estimated from the absorbance at 280 nm, assuming $E_{1\,cm}^{1\%}$ = 4.53 calculated from modified absorption coefficient of the residues (*19*).

Table 1. **Data collection and refinement statistics.**

Crystal data statistics	
Wavelength (Å)	0.8000
Data-collection temperature (K)	100
Space group	$P2_1$
Unit-cell parameters	a = 42.400 Å, b = 76.868 Å, c = 42.774 Å, β = 115.08°
Resolution range (Å)	30–1.34 (1.39–1.34)
Measured reflections	20,1760
Unique reflections	55,454
$I/\sigma(I)$	14.1 (3.6)
Completeness (%)	99.6 (100.0)
R_{merge} (%)	4.5 (35.6)
Refinement statistics	
R_{cryst} (%)[a]	20.3 (25.5)
R_{free} (%)[b]	22.1 (27.1)
No. of molecules per asymmetric unit	1
No. of protein atoms	1,860
No. of solvent molecules	303
Rmsd from ideality	
Bonds (Å)	0.007
Angles (deg.)	1.5
Coordinate error from Luzzati plot (Å)	0.16 (0.18)
Ramachandran plot, residues in (%)	
Favoured regions	97.0
Allowed regions	3.0
Generous regions	0.0
Disallowed regions	0.0

Values in parentheses are for the highest resolution shell.
[a]R_{cryst} was calculated from the working set (95% of the reflection data).
[b]R_{free} was calculated from the test set (5% of the reflection data).

Crystallization and Data Collection—Crystals of the *Tt*-α-subunit were obtained at 291 K using the oil batch method by TERA (*20*). A 0.5 μl aliquot of protein solution (28.27 mg/ml protein, 20 mM Tris-HCl, pH 8.0, 0.2 M NaCl) was mixed with an equal volume of reservoir solution (0.17 M ammonium acetate, 85 mM Citrate-NaOH, pH 5.6, 25.5% (w/v) polyethylene glycol 4000, 15% (v/v) glycerol) and covered with 15 μl of paraffin oil. After one week, crystals grew to a typical size of 0.1 × 0.1 × 0.15 mm. These crystals belonged to the space group $P2_1$ with a monomer in an asymmetric unit, and their solvent content and specific volume V_m (*21*) were 40.1% and 2.07 Å^3/Da, respectively. For data collection, these crystals were flash-cooled in a 100 K dry nitrogen stream. The data set was collected at the beamline BL26B1 of SPring-8, Japan. These data were processed with the programs DENZO and SCALEPACK (*22*). The statistics for the data collection are summarized in Table 1.

Structure Determination and Refinement—The structure was determined by the molecular replacement method using the program CNS (*23*). Chain B of the α-subunit from *Pyrococcus furiosus* (*Pf*-α-subunit) (PDB ID, 1GEQ) was used as the search model. Refinement was carried out using the program CNS. The structure was visualized and

revised using the program QUANTA (Accelrys Inc.). The refinement statistics are summarized in Table 1.

Calculation of Hydrophobic Interactions—The change in denaturation Gibbs energy (ΔG) due to hydrophobic effects between the wild-type and mutant proteins ($\Delta\Delta G_{HP}$) could be expressed using changes in accessible surface area (*ASA*) of nonpolar and polar atoms due to denaturation (*24*),

$$\Delta\Delta G_{HP} = 0.178\Delta\Delta ASA_{nonpolar} - 0.013\Delta\Delta ASA_{polar}, \quad (1)$$

where $\Delta\Delta ASA_{nonpolar}$ and $\Delta\Delta ASA_{polar}$ represent the differences in ΔASA of nonpolar and polar atoms of all residues in a protein, respectively, upon denaturation between wild-type and mutant proteins. *ASA* values of proteins in the native state can be calculated from their X-ray crystal structures, and those in the denatured state from their extended structures. For the calculation of *ASA*, C/S atoms in residues were assigned to $ASA_{nonpolar}$ and N/O to ASA_{polar}. *ASA* values using the X-ray crystal structure of the *Tt*-α-subunits in the native state were calculated according to the reported procedure (*25*). The *ASA* values in the denatured states were calculated from the extended structures, which were generated from the native structures using the program InsightII (Accelrys Inc.).

Calculation of Normalized B-Factor—The *B*-factor of each protein was normalized to compare the *B*-factors between different proteins by equation 2 (*26*),

$$B' = (B - \langle B\rangle)/\mathrm{sigma}(B), \quad (2)$$

where "B'", "B", "$\langle B\rangle$" and "sigma (B)" indicate the normalized *B*-factor, the *B*-factor of the main chain, the averaged *B*-factor of the main chains, and the standard deviation of the *B*-factors, respectively.

Differential Scanning Calorimetry—DSC was carried out with differential scanning calorimeters, MicroCal VP-DSC and VP-capillary DSC platform (Northampton). Prior to measurement, the protein solution was dialyzed against the buffer used. The dialyzed sample was filtered through a 0.22-μm pore size membrane and then degassed in a vacuum. The buffers used were 20 mM glycine-HCl in the acidic region, 30 mM phospahte-KOH in the neutral region and 20 mM glycine-KOH in the alkaline region. The protein concentrations under measurement were 0.3–1.2 mg/ml. The DSC curves were analyzed using Origin software from MicroCal (Northampton).

RESULTS

Thermal Stability of the α-Subunit of Tryptophan Synthase from T. thermophilus—To examine the thermal stability of the *Tt*-α-subunit, DSC measurements were carried out at various pH values. Figure 1 shows the pH dependency of the denaturation temperature of the *Tt*-α-subunit at a scan rate of 1°C/min. The denaturation temperature of the *Tt*-α-subunit was about 15°C higher than that of the *St*-α-subunit at pH 9.5 (*27*), and about 17°C lower than that of the *Pf*-α-subunit (*16*). In Fig. 2, the specific enthalpy changes upon denaturation (ΔH, the enthalpy change per a gram of protein) obtained from the peak area on the DSC curves of the *Tt*-α-subunit at various pH values are plotted against the denaturation temperature. Line (a) represents a least-square fit to the

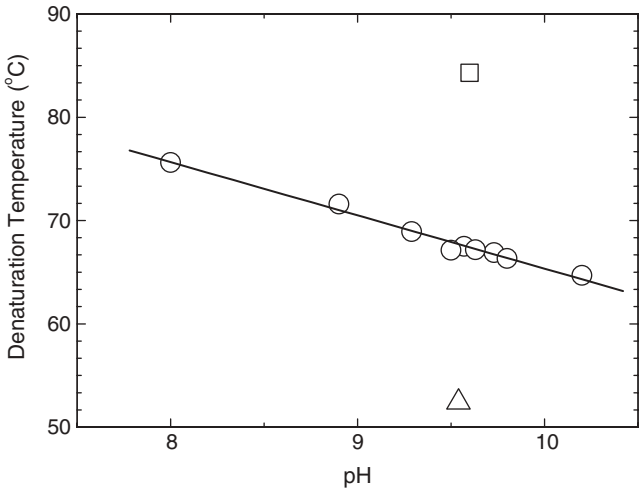

Fig. 1. **pH dependency of the denaturation temperatures of the *Tt*-α-subunit.** The denaturation temperature represents the peak temperatures of DSC curves. Square, circles, and triangle represent denaturation temperatures of the *Pf*-, *Tt*-, and *St*-α-subunits, respectively. DSC measurements were performed at a scan rate of 60°C/h. The line shown was obtained by a least-squares fit to the experimental points of the *Tt*-α-subunit at various pH. The denaturation temperatures at pH 9.5 of the *Pf*- and *St*-α-subunits were obtained in previous studies (*16*, *27*).

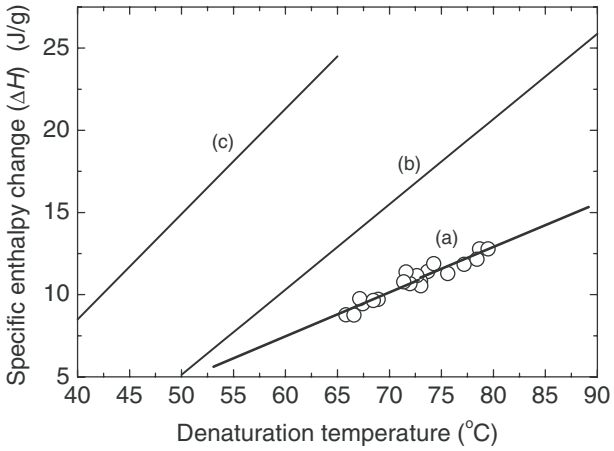

Fig. 2. **Specific enthalpy change upon denaturation for tryptophan synthase α-subunits as a function of denaturation temperature.** The circles represent experimental points of the *Tt*-α-subunit obtained at scan rate of 60°C/h and at various pHs. Line (a) was obtained by a least-squares fit to experimental points of the *Tt*-α-subunit. Lines (b) and (c) are the reported values for the *Pf*- and *St*-α-subunits, respectively (*16*, *27*).

experimental points. The slope corresponds to the change in specific heat capacity upon denaturation (ΔCp). The ΔCp value (0.28 J K^{-1} g^{-1}) of the *Tt*-α-subunit was less than those for the *Pf*-α-subunit (0.52 J K^{-1} g^{-1}) (*16*) and the *St*-α-subunit (0.64 J K^{-1} g^{-1}) (*27*). As shown in the figure, ΔH values of the *Tt*-α-subunit were remarkably lower than those of the other two proteins: they were 7.4 J/g, 10.3 J/g (*16*) and 21.4 J/g (*27*) at 60°C for the *Tt*-, *Pf*-, and *St*-α-subunits, respectively.

The second DSC scan of the *Tt*-α-subunit after heating and cooling at pH 9.0 did not show any excess heat capacity on the DSC curve, indicating that the heat denaturation of

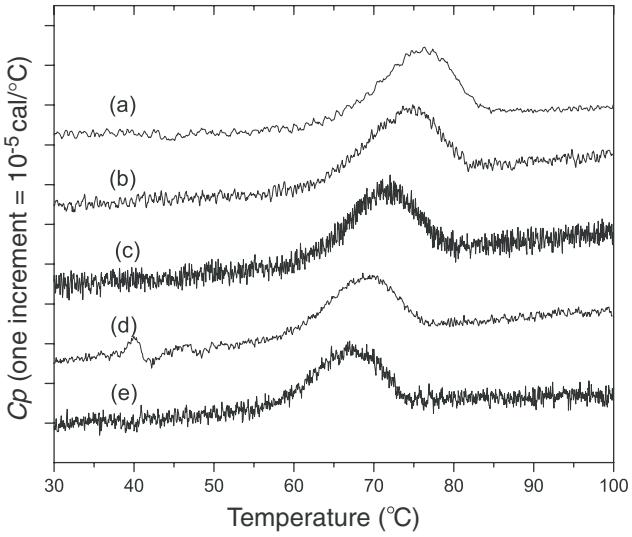

Fig. 3. **Dependence of excess heat capacity curves of the *Tt*-α-subunit on scan rates.** Samples at the same concentration (0.5 mg/ml) at pH 9.0 were measured at different scan rates. Curves (a) to (e) represent DSC curves at scan rates of 200, 120, 60, 30, and 15°C/h, respectively. As a feedback mode gain of VP-capillary DSC platform, "H" and "M" were used for measurements at scan rates of over 60°C/h and below 30°C/h, respectively. The *Cp* values normalized for protein concentration are presented.

the protein is not reversible under the conditions examined. Furthermore, the effect of scan rate on the DSC curves was examined at the same concentration (0.5 mg/ml) of the *Tt*-α-subunit. The scan rates examined were 15, 30, 45, 60, 85, 120, 150, and 200°C/h. As shown in Fig. 3, the peak temperatures at 15 and 30°C/h were clearly different, suggesting that the rate of heat denaturation is slower at these scan rates, and that the heat denaturation of the *Tt*-α-subunit is under kinetic control. Therefore, the parameters obtained from these DSC experiments are not equilibrium but kinetic values. A possible interpretation of this observation is that slow denaturation is preferable for the function of this protein at high temperature, as pointed out in the thermodynamic study of pyrrolidone carboxyl peptidase from the hyperthermophile *P. furiosus* (*28*).

Quality of the Model and Overall Structure for the Tt-α-Subunit—The refinement of the *Tt*-α-subunit converged to an R_{cryst} of 20.3% and an R_{free} of 22.1% for the reflections in resolution range of 30–1.34 Å. The refined model consisted of 1,860 protein atoms, a citrate in the active site, and 303 water molecules. Electron density was not observed for the flexible loops comprising of residues 55–58, 177–188, and 257–268. The model of the *Tt*-α-subunit converged well to ideal bond lengths and angles with rmsd values of 0.007 Å and 1.5°, respectively. In the Ramachandran plot, 97.0% of the non-glycine residues were in the most favorable region, 3.0% in the additionally allowed region, and no residue was in the generous or the disallowed regions. The final coordinates have been deposited in the Protein Data Bank (accession No. 1UJP).

The structure of the *Tt*-α-subunit is illustrated as a ribbon drawing and an α-carbon trace in Figures 4A and 4B, respectively. The topology of the *Tt*-α-subunit was an 8-fold α/β (TIM) barrel fold with three extra helices, which is similar to those of the α-subunit orthologs from other sources (*16*, *17*). The three C-terminal residues were trapped in a hydrophobic pocket of the neighboring subunit in the crystal (Fig. 4B and C). Electron density for these three residues (269Pro-270Leu-271Pro) was clearly observed as shown in Fig. 4C. However, the structures of the C-terminal residues, 257–268, could not be determined due to the lack of significant electron density. Dynamic light scattering measurements (DynaPro MS/X) suggested that the *Tt*-α-subunit is a monomer in solution at pH 7.8 (data not shown). Therefore, the C-terminal 15 residues (257–271) might be flexible in solution.

The most important catalytic base of the *St*-α-subunit is Glu49, and Asp60 is a second catalytic base (*29*, *30*). The corresponding residues in the *Tt*-α-subunit are Glu47 and Asp58, respectively. Glu47 of the *Tt*-α-subunit is located in nearly the same position as that in the *St*-α-subunit, but the position of the Asp58 could not be determined due to poor electron density.

Structural Comparison of the Tt-α-Subunit with the Other Two α-Subunits—The secondary structure-based sequence alignments of the three α-subunit orthologs were performed based on the assignment by DSSP (*31*) (Fig. 5). The alias of secondary structure segments of the *St*-α-subunit named by Hyde *et al*. (*17*) can be used for those of the *Tt*-α-subunit. All the secondary segments of the three proteins are conserved except for helix-0, which is missing in the *Pf*-α-subunit. A long flexible loop in the C-terminus of the *Tt*-α-subunit is not found in the other two proteins.

The *Tt*-α-subunit shows sequence identities with the *Pf*-α-subunit and *St*-α-subunit of 40% and 27%, respectively. The average rmsd values of equivalent Cα atoms were calculated to be 2.20 Å between the *Tt*- and *Pf*-α-subunits and 2.33 Å between the *Tt*- and *St*-α-subunits. These values were smaller than the reported rmsd value of 2.82 Å between the *Pf*- and the *St*-α-subunits (*16*). The rmsd values of Cα atoms for equivalent residues along the chain between the *Tt*-α-subunit and *Pf*-α-subunit, and between the *Tt*-α-subunit and the *St*-α-subunit are plotted in Fig. 6 (a) and (b), respectively. Several significant deviations over 3 Å are found. The peak Ia of deviation is caused by twelve missing residues in the N-terminus of the *Pf*-α-subunit. By contrast, the N-terminal structure of the *Tt*-α-subunit is similar to that of the *St*-α-subunit, so that the large deviation is limited only to the N-terminal residue (peak Ib). The residues corresponding to Glu41 and Ile95 of the *St*-α-subunit were missing in the *Tt*-α-subunit and the *Pf*-α-subunit (Figs 5 and 6), resulting in the peaks IIb and IIIb. These deletions resulted in the shortening of loop regions (between helix-1 and strand-2, and between helix-2 and strand-3), which might be correlated with the thermostability of both proteins (the *Pf*-α-subunit and the *Tt*-α-subunit) from the thermophiles. The residues belonging to peaks IIa and IVb correspond to those interacting with the β_2-subunit in the *St*-$\alpha_2\beta_2$ complex. This region, which is the loop between strand-4 and helix-4, was found to be more mobile when the *B*-factors of the *Tt*-α-subunit were compared with those of the *St*-α-subunit in the complex form (Fig. 7). The conformations for these regions might be tuned to that seen in the *St*-α-subunit when the α-subunit forms the complex with the β_2-subunit. There are

two possibilities as to why the rmsd values for IIa (between *Tt* and *Pf*) and IVb (between *Tt* and *St*) are different. The first is that the conformation of this region in the *Tt*-α-subunit was accidentally trapped by crystal packing to that of the complex form in the *St*-α-subunit. The other possibility is that the structure of this region might be essentially different between Eubacterium and Archaebacterium. The electron density of residues 177–188 in

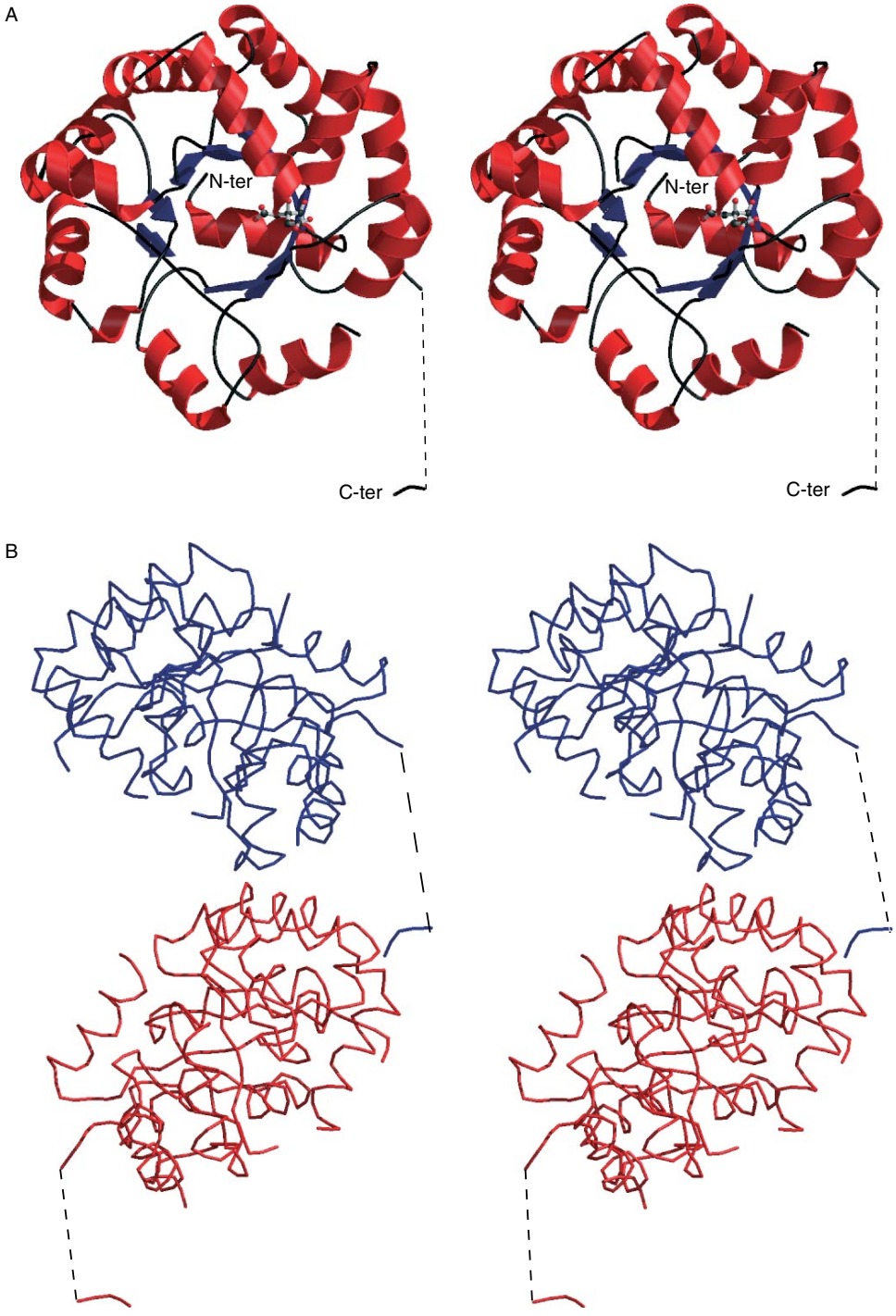

Fig. 4. **The structure of the α-subunit of tryptophan synthase from *Thermus thermophilus*.** (A) Schematic stereo view of the *Tt*-α-subunit. The figure was prepared using the program Molscript (*46*) and Raster3D (*47*). The dotted line represents the disordered region at the C-terminus. (B) Stereo drawings of the *Tt*-α-subunit (blue) and its symmetry-related molecule (red) interacting with the C-terminal residues. The dotted line represents the disordered region at the C-terminus. (C) C-terminal structure of the *Tt*-α-subunit interacting with the symmetry-related molecule. The $2F_o$–F_c electron density is shown at 1σ contouring. The blue and red represent C-terminal residues (Pro269-Leu270-Pro271) of the *Tt*-α-subunit and its symmetry-related molecule, respectively. These figures were prepared by the program Quanta 2000 (Accelrys Inc.).

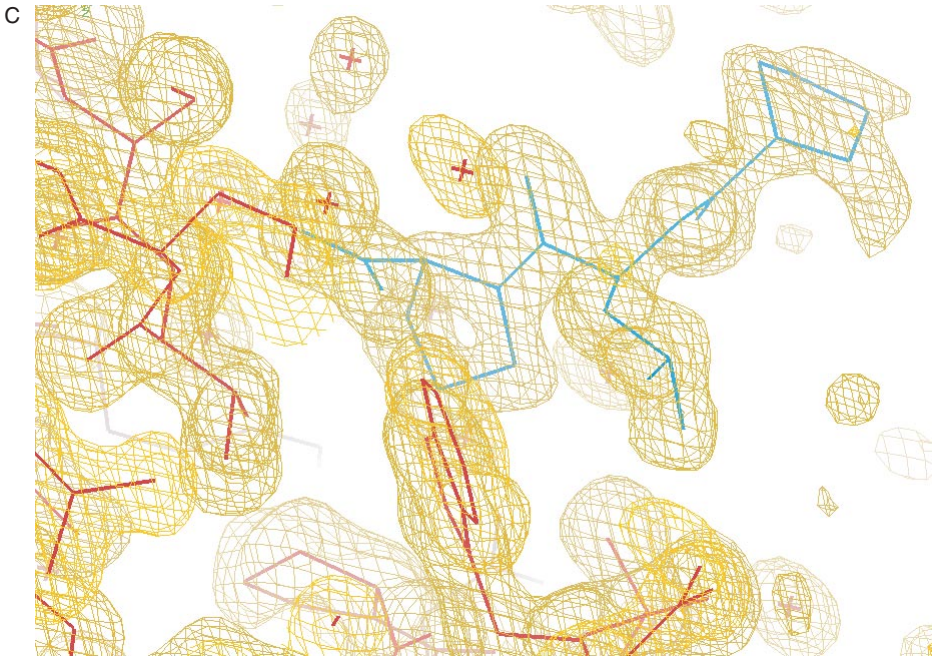

Fig. 4. Continued.

the long loop region between strand-6 and helix-6 was not observed in the *Tt*-α-subunit. The peaks IIIa and Vb correspond to helix-6. The N-terminal side of helix-6 was more deviated, affected by the mobility of the long flexible loop. The peaks IVa (VIb) and Va (VIIb) might be a consequence of the occurrence of two residues in helix-7 and five residues in helix-8 (and/or helix-8′) in the *Tt*-α-subunit, which are shortened as compared with those of the *Pf*- and *St*-α-subunits. Ignoring the long flexible loop at the C-terminus, seven and nine residues of the *Tt*-α-subunit were deleted as compared to the *Pf*- and *St*-α-subunits, respectively, within the TIM barrel fold (from strand-1 to helix-8).

The total numbers of hydrogen bonds for the *Tt*-, *Pf*-, and S*t*-α-subunits were 144 from 271 residues, 145 from 248 residues, and 144 from 268 residues, respectively (Table 2), indicating nearly the same numbers of hydrogen bonds. On the other hand, the total numbers of the ion pairs within 4 Å for the *Tt*-, *Pf*-, and *St*-α-subunits were 28, 22, and 20, respectively (Table 2). The total numbers of ion pairs for the *Tt*-, and *Pf*-α-subunits were greater than in the *St*-α-subunit, indicating that thermophile proteins have greater numbers of ion pairs (salt bridges).

A decrease in cavity volume in the hydrophobic core has been reported as one of the key factors for the thermal stability of proteins (*13*). The cavity volume was determined using a probe radius of 1.4 Å (*25*). The energy term ΔG due to changes in the cavity size can be calculated using the reported parameter of 52 J mol^{-1} $Å^{-3}$ (*32*). The cavity volumes in the *Tt*-, *Pf*- and *St*-α-subunits were 250.3 Å, 226.8 $Å^3$, and 318.1 $Å^3$, respectively, and ΔG values were estimated to be −13.0 kJ/mol, −11.8 kJ/mol, and −16.5 kJ/mol, respectively (Table 2). This result indicates that the decrease in cavity size contributes to the conformational stability of the α-subunits from thermophilic organisms.

DISCUSSION

Contribution of Hydrophobic Interaction—The hydrophobic interaction is one of the important stabilizing forces of folded protein structure (*33*). Takano *et al.* (*34*) have found a general rule for the relationship between hydrophobic effect and conformational stability of proteins using a series of hydrophobic mutants of human lysozyme. The contribution of the hydrophobic interaction was estimated for the *Tt*-α-subunit using equation 1 of "MATERIAL AND METHODS." As shown in Table 2, the ΔG values arising from hydrophobic interactions in the *Tt*-α-subunit were 131.1 kJ/mol and 211.1 kJ/mol lower than those of the *Pf*- and *St*-α-subunits, respectively. This means that the contribution of hydrophobic interaction to the conformational stability of the *Tt*-α-subunit is not greater than those of the *St*- and *Pf*-α-subunits (*16*).

Makhatadze and Privalov (*35*) have reported that protein folding is an enthalpically driven process caused by van der Waals interactions between nonpolar groups in the interior of proteins. In the case of the *Tt*-α-subunit, enthalpic effects did not cause higher stability, suggesting that the hydrophobic interactions due to nonpolar groups in the interior of the protein are not as dominant as those of the *Pf*- and S*t*-α-subunits. This indicates that experimental results from DSC agree with analytical results of hydophobic interaction on the basis of tertiary structures.

Thermo-Stabilization Mechanism of the Tt-α-Subunit—Because the denaturation temperature of the *Tt*-α-subunit under equilibrium conditions could not be determined, we cannot compare the Gibbs energy curves of denaturation as a function of temperature with those of the *Pf*- and *St*-α-subunits. However, the present results from calorimetry indicate that the ΔH and ΔCp values of denaturation for the *Tt*-α-subunit are remarkably lower than those of the other two proteins, although the denaturation temperatures

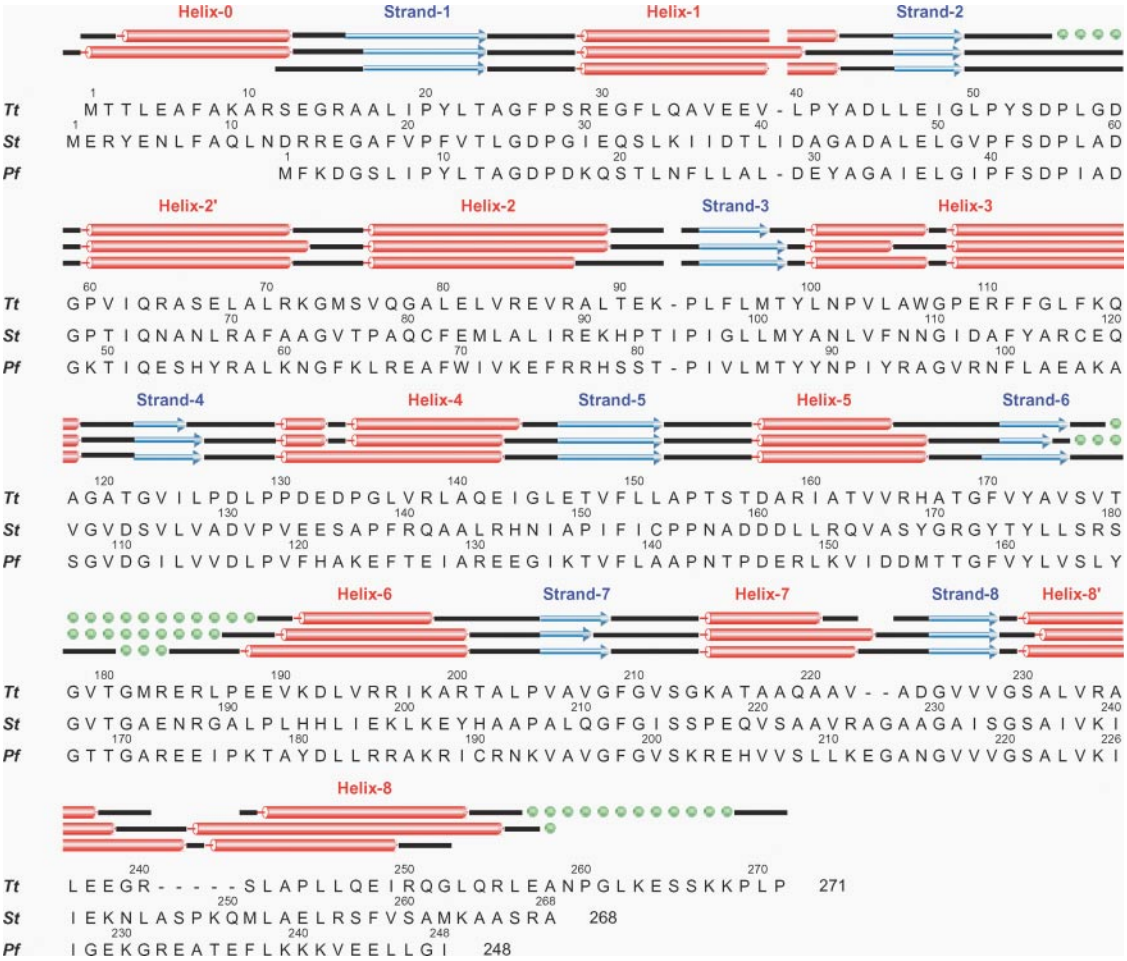

Fig. 5. **Sequence alignments using the secondary structures of the *Tt*-, *Pf*-, and *St*-α-subunits.** The first line represents the alias of the secondary segments named by Hyde *et al*. (*17*). The second, third, and forth lines represent the secondary structural elements of the *Tt*-, *St*-, and *Pf*-α-subunits, respectively, based on the secondary structure definition as established by the program DSSP (*31*). Red blocks, blue arrows, black bars, green balls, and spaces represent helices including 3_{10}-helices, β-strands, the other structures, disordered (no electron density), and missing residues, respectively. The fifth, seventh, and ninth lines represent residue numbers of the *Tt*-, *St*-, and *Pf*-α-subunits, respectively. The sixth, eighth, and tenth lines represent amino acid sequences of the *Tt*-, *St*-, and *Pf*-α-subunits, respectively.

around pH 9 are intermediate to those of the *Pf*- and *St*-α-subunits.

When the Δ*H* values of the protein, which is more stable, are lower than those of the others, thermo-stabilization should be caused by entropic effects ($\Delta G = \Delta H - T\Delta S$). The higher stability of the *Pf*-α-subunit has been reported to be caused by entropic factors as compared with the *St*-α-subunit (*16*). In the case of the *Tt*-α-subunit, its stability might be due to entropic effects relative to the *St*-α-subunit, and destabilized by enthalpic effects relative to the *Pf*-α-subunit. Lowering the denaturation entropy of a protein is one way of increasing its stability. For example, substitution by the less flexible residue Pro (*36*–*38*) and the introduction of a disulfide bond (*39*) can increase the stability of proteins. Shortening the polypeptide chain can also lower the conformational entropy of a protein in the denatured state. For thermophile proteins, a shortening of the N and C termini and a reduction of loop sizes have been observed (*4*, *15*, *16*, *40*, *41*).

The number of Pro residue for the *Tt*-α-subunit is 20, and greater than those of the other two proteins (Table 3), suggesting the contribution to decreasing the entropy of the *Tt*-α-subunit in the denatured state. From sequence alignments of the secondary structures among the three proteins (Fig. 3), deletions of nine residues at four positions of the *Tt*-α-subunit were found. Two positions (corresponding to Ile41 and Ile95 of the *St*-α-subunit) were deleted in both thermophiles, suggesting that these reductions in loop size contribute to the stabilization of the *St*- and *Pf*-α-subunits. The deletions at the other two positions shorten the C-termini of α-helices (helix-7 and helix-8′). In the C-terminus, the *Pf*-α-subunit lacks six residues compared with the *St*-α-subunit, but in the *Tt*-α-subunit, the C-terminus is extended by sixteen residues, so it does not possess a defined structure in the crystal and is mostly composed of hydrophilic amino acids. The role of these extended residues, which are not favorable to protein stability, can not be interpreted. Oobatake and Ooi (*42*) have estimated the contribution to the thermodynamic parameters upon denaturation of each amino acid residue. Using these parameters (Table 3), the contribution to Gibbs energy due to conformational entropy upon denaturation

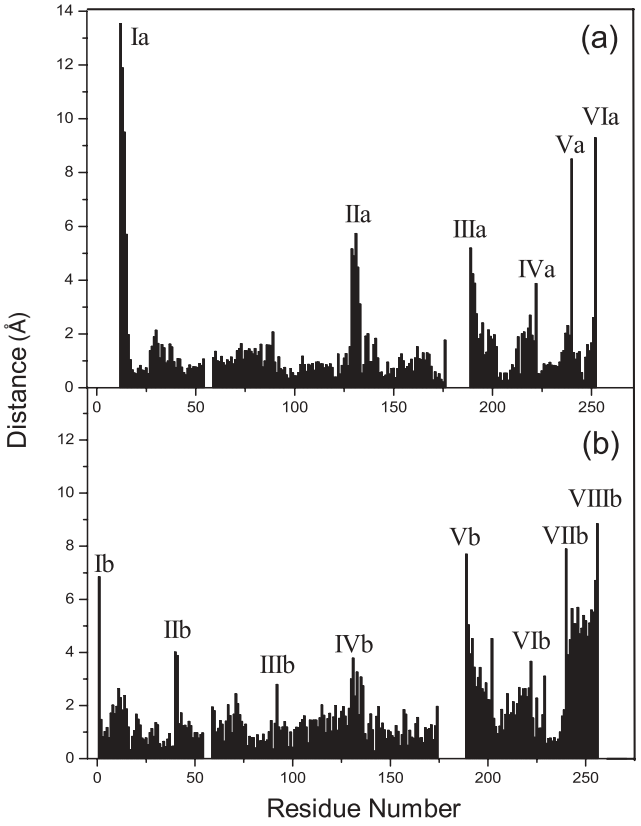

Fig. 6. **Rmsd of Cα atoms between the *Tt*- and *Pf*-α-subunits (a) and between the *Tt*- and *St*-α-subunits (b) after least square fitting of corresponding Cα atoms.** Peaks Ia to VIa and Ib to VIIIb represent segments of large differences over 3 Å. Residue numbers for the *Tt*-α-subunit are shown.

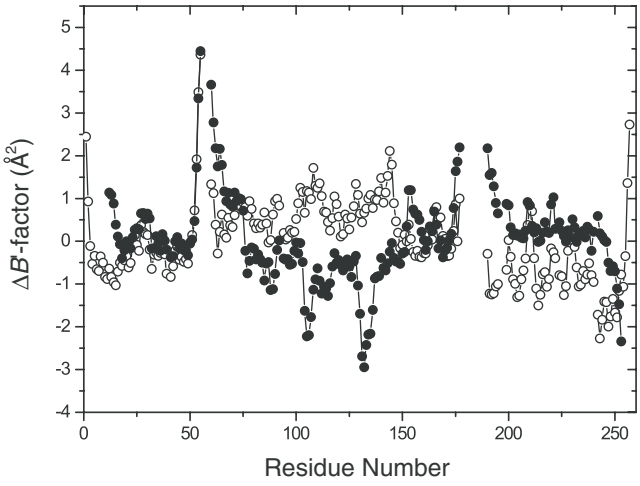

Fig. 7. **Differences in normalized *B*-factors (Å²) for the main-chain atoms *versus* residue number between the *Tt*- and *Pf*-α-subunits (closed circles) and between the *Tt*- and *St*-α-subunits (open circles).** Δ*B*′-factors are the differences in normalized *B*-factors of the α-subunit in the *St*-$\alpha_2\beta_2$-complex (1BKS) or the *Pf*-α-subunit from those of the *Tt*-α-subunit. The *B*-factor of each protein was normalized using equation 2 to facilitate the comparison of the *B*-factors between different proteins (*26*). Residue numbers for the *Tt*-α-subunit are shown.

Table 2. **Estimate of the difference in stability of three tryptophan synthase α-subunits on the basis of structural information.**

	Tt-α-subunit	*Pf*-α-subunit	*St*-α-subunit
Hydrophobicity			
Δ*ASA* (C/S)	15,878.7 Å^2	16,449.0 Å^2	16,918.0 Å^2
Δ*ASA* (N/O)	6,829.7 Å^2	6,953.0 Å^2	7,214.0 Å^2
Δ*G*	2,705.9 kJ/mol	2,873.3 kJ/mol	2,917.1 kJ/mol
ΔΔ*G*	–	131.4 kJ/mol	211.2 kJ/mol
Cavity volume			
Cavity vol. (probe 1.4 Å)	250.3 Å^3	226.8 Å^3	318.1 Å^3
Δ*G*	–13.0 kJ/mol	–11.8 kJ/mol	–16.5 kJ/mol
ΔΔ*G*	–	1.2 kJ/mol	–3.5 kJ/mol
Hydrogen bond	144	145	144
Ion pair (within 4 Å)	28	22	20
Ion pair (within 5 Å)	50	48	41
Total number of residues	271	248	268
TΔ*S* at 25°C	72.2 kJ/mol	190.2 kJ/mol	205.9 kJ/mol

ΔΔ*G* represents the difference in Δ*G* between *Tt* and *Pf*, *Tt* and S*t*, respectively.

(TΔ*S*) at 25°C were estimated to be 72.2, 190.2, 205.9 kJ/mol, for the *Tt*-, *Pf*-, and *St*-α-subunits, respectively (Table 2). These results suggest that the remarkably smaller denaturation entropy of the *Tt*-α-subunit contributes to its conformational stability as compared with the other two proteins, in agreement with the calorimetric results.

Robic *et al.* (*43*) have proposed that the lower Δ*Cp* value of ribonuclease H from the thermophilic bacterium *T. thermophilus* contributes to its higher stability, and that it originates from residual structures in the denatured state; the residual structures decrease entropy in the denatured state. The Δ*Cp* value of the *Tt*-α-subunit (0.28 J K^{-1} g^{-1}) is lower than those of the *Pf*-α-subunit (0.52 J K^{-1} g^{-1}) and the *St*-α-subunit (0.64 J K^{-1} g^{-1}). If we assume that this lower Δ*Cp* value of the *Tt*-α-subunit, which is from the same source as the above ribonuclease H, is derived from the residual structures in the denatured state, the lower Δ*Cp* value is relevant to the smaller denaturation entropy, thereby suggesting its contribution to the higher stability.

Stability Analysis of the α-Subunit Structure by Knowledge Based Potential—Ota *et al.* (*44*) have proposed that the changes in conformational stability due to single amino acid substitution can be calculated by SPMP (Stability Profiles of Mutant Proteins) based on the native structures. In SPMP calculations, the pseudo-energy potential ($\Delta\Delta G_{SPMP}$) developed for fold recognition is employed. It consists of four elements: side-chain packing ($\Delta\Delta G_{SP}$), hydration ($\Delta\Delta G_{Hyd}$), local structure ($\Delta\Delta G_{LC}$), and backbone-sidechain repulsion ($\Delta\Delta G_{BR}$) (*44*, *45*).

$$\Delta\Delta G_{SPMP} = \Delta\Delta G_{SP} + \Delta\Delta G_{Hyd} + \Delta\Delta G_{LC} + \Delta\Delta G_{BR} \quad (3)$$

The pseudo-energy potential provides a fitness score for each residue type at a site in the native structure.

Table 3. **Estimated denaturation entropy of each α-subunit from its amino acid composition.**

	α-Subunit from *T. thermophilus* HB8			α-Subunit from *P. furiosus*			α-Subunit from *S. typhimurium*		
	Number of residues	Percentage	ΔSu (J mol^{-1} K^{-1})	Number of residues	Percentage	ΔSu (J mol^{-1} K^{-1})	Number of residues	Percentage	ΔSu (J mol^{-1} K^{-1})
Hydrophobic	166	61.3	1,290.9	133	53.7	1,332.5	157	58.6	1,440.4
Gly	25	9.3	–112.4	21	8.5	–94.4	20	7.5	–89.9
Ala	34	12.6	259.9	22	8.9	168.2	40	15.0	305.8
Val	26	9.6	131.1	21	8.5	105.9	17	6.4	85.7
Leu	38	14.1	129.3	25	10.1	85.1	28	10.5	95.3
Ile	8	3.0	30.0	17	6.9	63.6	18	6.8	67.3
Met	4	1.5	133.3	3	1.3	100.0	5	1.9	166.6
Phe	10	3.7	656.9	13	5.3	854.0	12	4.5	788.3
Trp	1	0.4	37.8	1	0.5	37.8	0	0.0	0
Pro	20	7.4	25.2	10	4.1	12.6	17	6.4	21.5
Neutral	38	14.1	–144.5	35	14.2	–65.2	47	17.6	–227.7
Ser	12	4.5	42.4	11	4.5	38.9	16	6.0	56.5
Thr	15	5.6	56.1	14	5.7	52.4	7	2.7	26.2
Asn	2	0.8	–49	7	2.9	–171.5	11	4.2	–269.4
Gln	9	3.4	–194	2	0.9	–43.1	10	3.8	–215.5
Cys	0	0.0	0.0	1	0.5	58.2	3	1.2	174.6
Hydrophilic	67	24.8	–904.4	80	32.3	–629.4	64	23.9	–522.5
Asp	9	3.4	32.6	12	4.9	43.4	13	4.9	47.0
Glu	22	8.2	60.1	20	8.1	54.6	16	6.0	43.7
Lys	10	3.7	–158.8	20	8.1	–317.6	8	3.0	–127.1
His	1	0.4	3.2	4	1.7	12.6	5	1.9	15.8
Arg	20	7.4	–1040	15	6.1	–780.0	15	5.6	–780
Tyr	5	1.9	198.7	9	3.7	357.6	7	2.7	278.2
Total number	271	100.0	242.1	248	100.0	638	268	100.0	690.2
TΔ*S* (kJ mol^{-1}) at 25°C		72.2			190.2			205.9	

ΔSu represents denaturation entropy obtained using the parameters of Oobatake and Ooi (*42*).

The estimation of ΔΔ*G* for the replacement of residue X by residue Y is as follows.

$$\Delta\Delta G(\mathrm{X}\rightarrow\mathrm{Y}) = \Delta G(\mathrm{Y}) - \Delta G(\mathrm{X}) = [G^D(\mathrm{Y}) - G^N(\mathrm{Y})] - [G^D(\mathrm{X}) - G^N(\mathrm{X})] = [G^D(\mathrm{Y}) - G^D(X)] - [G^N(\mathrm{Y}) - G^N(\mathrm{X})] \quad (4)$$

where $G^{\mathrm{N}}(\mathrm{X})$ represents the Gibbs energy of the residue X at any structural site in the native protein molecule. The corresponding energy for the denatured state, $G^{\mathrm{D}}(\mathrm{X})$, is defined as the energy of residue X in a random environment (*44*).

The conformational stabilities of the three α-subunit structures were analysed by SPMP. The individual stability score for the four terms are summarized in Table 4. The total score correlates strongly with the experimentally obtained denaturation temperatures (Fig. 8). The score differences of *Pf*-α-subunit and *Tt*-α-subunit from *St*-α-subunit, *e.g.*, *Pf–St* and *Tt–St*, indicate significant stability of the former two. The *Pf*-α-subunit appears to be stabilized mainly by the side-chain packing term, while the hydration and side-chain packing terms can stabilize the *Tt*-α-subunit. These results indicate that the thermostabilization mechanisms of the *Pf*- and *Tt*-α-subunits, relative to the *St*-α-subunit, are different from each other. Furthermore, SPMP calculation provides stability scores for any residue substitution at any site. For example, in the case of the *Tt*-α-subunit with 243 amino acid residues, ΔΔ*G* values for 243 × 19 mutants were predicted by SPMP (*44*) using the crystal structure. If we consider the SPMP ranking at any site composed of a wild-type and 19 mutant amino acids, the structural stability defined by the wild-type sequence can be evaluated by the average ranking of wild-type residues at all sites. Actually, the average rankings of wild-type residues for the *Pf*-, *Tt*-, and *St*-α-subunits were calculated as 4.78, 5.10, and 5.24, respectively, corresponding to the order of the experimentally obtained

Table 4. **SPMP stability scores of α-subunits of tryptophan synthase.**

	Total	SP	Hyd	LC	BR
Tt	141.36	95.64	22.13	40.80	–17.20
Pf	151.43	111.26	20.08	36.72	–16.58
St	131.15	89.93	18.52	39.11	–16.50
Pf–St	20.28	21.33	1.56	–2.39	–0.08
Tt–St	10.21	5.71	3.61	1.69	–0.70

Unit is kJ/mol. Positive values indicate stabilization. *Pf–Tt* and *St–Tt* represent the difference in total scores between *Pf* and *Tt*, and between *St* and *Tt,* respectively. SP, Hyd, LC, and BR are contributions due to side-chain packing ($\Delta\Delta G_{\mathrm{SP}}$), hydration ($\Delta\Delta G_{\mathrm{Hyd}}$), local structure ($\Delta\Delta G_{\mathrm{LC}}$) and backbone-sidechain repulsion ($\Delta\Delta G_{\mathrm{BR}}$), respectively (Eq. 3).

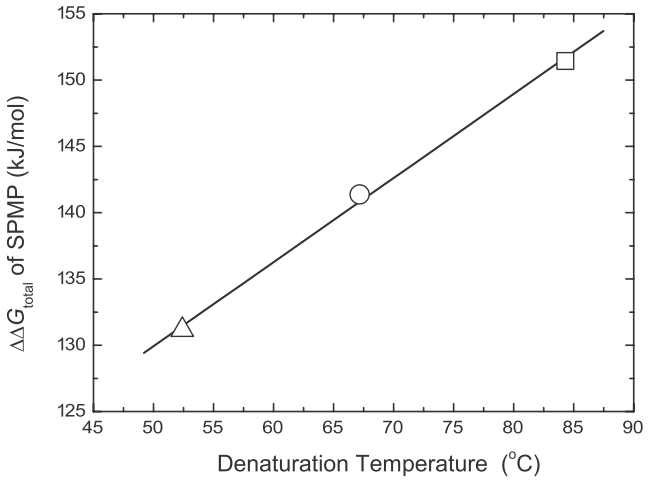

Fig. 8. **Relationship between total SPMP scores and denaturation temperatures of the three α-subunits.** The square, circle, and triangle represent denaturation temperatures of the *Pf*-, *Tt*-, and *St*-α-subunits at pH 9.5, respectively. The SPMP scores were obtained from Table 4.

stabilities of the proteins. Furthermore, the total SPMP score also shows a good correlation with the experimental denaturation temperature (Fig. 8). These results suggest that the most stable α-subunit with the lowest ΔG value upon folding can be assumed; the real proteins with wild-type sequences are less stable than the hypothetical most stable protein, and their stabilities are settled so as to be preferable for their biological environment.

CONCLUSIONS

The crystal structure of the *Tt*-α-subunit was determined at 1.34 Å resolution. The stability was examined using DSC. The denaturation temperature of the *Tt*-α-subunit at pH 9.5 was higher than that of the *St*-α-subunit but lower than that of the *Pf*-α-subunit. Specific denaturation enthalpy and specific denaturation heat capacity values of the *Tt*-α-subunit were the lowest among the three proteins, suggesting that entropy effects are responsible for the stabilization of the *Tt*-α-subunit. Heat denaturation was remarkably slow and was under kinetic control.

The structure of the *Tt*-α-subunit has a similar fold to the other orthlogs but an extension of thirteen residues at the C-terminus and deletion of four positions as compared with the *St*-α-subunit. Two deletions in loop regions seem to be responsible for the stabilization of the protein. As compared with the *St*-α-subunit, the increase in the number of ion pairs and decrease in the cavity volume might also contribute to the stabilization of the *Tt*-α-subunit. However, the numbers of hydrogen bonds were similar to the others, and the contribution of hydrophobic interactions was less.

In conclusion, the native structure of the *Tt*-α-subunit might be significantly better adapted to an ideally stable structure than that of the *St*-α-subunit, but worse than that of the *Pf*-α-subunit as shown by SPMP scores. The residual structure of the *Tt*-α-subunit in the denatured state might contribute to the stabilization, in agreement with the results of calorimetry.

Of authors, Y.A. solved the structure and wrote the paper, M.S., K.O., and J.N. performed the DSC experiments, M.O. analyzed SPMP scores, C.K. contributed the large-scale protein production, M.S. carried out the automated crystallization, and K.Y. and N.K. supervised the work. The authors would like to thank the technical staff of Advanced Protein Crystallography Research Group for assistance in the large-scale protein production and the automated crystallization. We also thank M.R.N. Murthy for critical reading of the manuscript, and the beamline staff for assistance during data collection at the beamline BL26B1 of SPring-8. The expression plasmid of the *Tt*-α-subunit (TT0017/HTPF00088) was supplied by the RIKEN Structurome Group, headed by S. Kuramitsu and S. Yokoyama. This work was supported by 'National Project on Protein Structural and Functional Analysis' funded by the Ministry of Education, Culture, Sports, Science and Technology of Japan.

REFERENCES

1. Jaenicke, R. and Bohm, G. (1998) Stability of proteins in extreme environments. *Curr. Opin. Struct. Biol.* **8**, 738–748
2. Chan, M.K., Mukund, S., Kletzin, A., Adams, M.W.W., and Rees, D.C. (1995) Structure of a hyperthermophilic tungstopterin enzyme, aldehyde ferredoxin oxidoreductase. *Science* **267**, 1463–1469
3. Britton, K.L., Baker, P.J., Borges, K.M., Engel, P.C., Pasquo, A., Rice, D.W., Robb, F.T., Scandurra, R., Satillman, T.J., and Yip, K.S. (1995) Insights into thermal stability from a comparison of the glutamate dehydrogenases from *Pyrococcus furiosus* and *Thermococcus litoralis*. *Eur. J. Biochem.* **229**, 688–695
4. Russell, R.J.M., Hough, D.W., Danson, M.J., and Taylor, G.L. (1994) The crystal structure of citrate synthase from the hyperthermophilic archaeon *Thermoplasma acidophlum*. *Structure* **2**, 1157–1167
5. Spassov, V.Z., Karshikoff, A.D., and Ladenstein, R. (1995) The optimization of protein-solvent interactions: thermostability and the role of hydrophobic and electrostatic interactions. *Protein Sci.* **4**, 1516–1527
6. Schumann, J., Bohm, G., Schumacher, G., Rudolph, R., and Jaenicke, R. (1993) Stabilization of creatinase from *Pseudomonas putida* by random mutagenesis. *Protein Sci.* **10**, 1612–1620
7. Tanner, J., Hecht, R.M., and Krause, K.L. (1996) Determinants of enzyme thermostability observed in the molecular structure of *Thermus aqaticus* D-glyceraldehyde-3-phosphate dehydrogenase at 2.5 Å resolution. *Biochemistry* **35**, 2597–2609
8. Henning, M., Darimont, B., Sterner, R., Kirschner, K., and Jansonius, J.N. (1995) 2.0 Å structure of indole-3-glycerol phosphate synthase from the hyperthermophile Sulfolobus solfataricus: possible determinants of protein stability. *Structure* **3**, 1295–1306
9. Korndorfer, I., Steipe, B., Huber, R., Tomschy, A., and Jaenicke, R. (1995) The crystal structure of holo-glyceraldehyde-3-phosphate dehydrogenase from the hyperthermophilic bacterium *Thermotoga maritima* at 2.5 Å resolution. *J. Mol. Biol.* **246**, 511–521
10. Yip, K.S.P., Stillman, T.J., Britton, K.L., Artymiuk, P.J., Baker, P.J., Sedelnikova, S.E., Engel, P.C., Pasquo, A., Chiaraluce, R., Consalvi, V., Scandurra, R., and Rice, D.W. (1995) The structure of *Pyrococcus furiosus* glutamate dehydrogenase reveals a key role for ion-pair networks in maintaining enzyme stability at extreme temperatures. *Structure* **3**, 1147–1158
11. Aguilar, C.F., Sanderson, I., Moracci, M., Ciaramella, M., Nucci, R., Rossi, M., and Pearl, L.H. (1997) Crystal structure of the β-glycodsidase from the hyperthermophilic archaeon *Sulfolobus solfataricus*: resilience a key factor in thermostability. *J. Mol. Biol.* **271**, 789–802

12. Henning, M., Sterner, R., Kirschner, K., and Jansonius, J.N. (1997) Crystal structure at 2.0 Å resolution of phosphoribosyl anthranilate isomerase from the hyperthermophile *Thermotoga maritima*: possible determinants of protein stability. *Biochemistry* **36**, 6009–6016
13. Knapp, S., de Vos, W.M., Rice, D., and Ladenstein, R. (1997) Crystal structure of glutamate dehydrogenase from the hyperthermophile eubacterium *Thermotoga maritima* at 3.0 Å resolution. *J. Mol. Biol.* **267**, 916–932
14. Russell, R.J.M., Ferguson, J.M.C., Hough, D.W., Danson, M.J., and Taylor, G.L. (1997) The crystal structure of citrate synthase from the hyperthermophilic archaeon *Pyrococcus furiosus* at 1.9 Å resolution. *Biochemistry* **36**, 9983–9994
15. Tahirov, T.H., Oki, H., Tsukihara, T., Ogasahara, K., Yutani, K., Ogata, K., Izu, Y., Tsunasawa, S., and Kato, I. (1998) Crystal structure of methionine aminopeptidase from hyperthermophile, *Pyrococcus furiosus*. *J. Mol. Biol*. **284**, 101–124
16. Yamagata, Y., Ogasahara, K., Hioki, Y., Lee, S.J., Nakagawa, A., Nakamura, H., Ishida, M., Kuramitsu, S., and Yutani, K. (2001) Entropic stabilization of the tryptophan synthase alpha-subunit from a hyperthermophile, *Pyrococcus furiosus*. X-ray analysis and calorimetry. *J. Biol. Chem*. **276**, 11062–11071
17. Hyde, C.C., Ahmed, S.A., Padlan, E.A., Miles, E.W., and Davies, D.R. (1988) Three-dimensional structure of the tryptophan synthase $\alpha_2\beta_2$ multienzyme complex from *Salmonella typhimurium*. *J. Biol. Chem.* **263**, 17857–17871
18. Yokoyama, S., Hirota, H., Kigawa, T., Yabuki, T., Shirouzu, M., Terada, T., Ito, Y., Matsuo, Y., Kuroda, Y., Nishimura, Y., Kyogoku, Y., Miki, K., Masui, R., and Kuramitsu, S. (2000) Structural genomics projects in Japan. *Nat. Struct. Biol*. **7**, 943–945
19. Pace, C.N., Vajdos, F., Fee, L., Grimsley, G., and Gray, T. (1995) How to measure and predict the molar absorption coefficient of a protein. *Protein Sci.* **4**, 2411–2423
20. Sugahara, M. and Miyano, M. (2002) *Tanpakushitsu Kakusan Koso* **47**, 1026–1032
21. Matthews, B.W. (1968) Solvent content of protein crystals. *J. Mol. Biol.* **33**, 491–497
22. Otwinowski, Z. and Minor, W. (1997) Processing of X-ray diffraction data collected in oscillation mode. *Methods Enzymol.* **276**, 307–326
23. Brünger, A.T., Adams, P.D., Clore, G.M., DeLano, W.L., Gros, P., Grosse-Kunstleve, R.W., Jiang, J.S., Kuszewski, J., Nilges, M., Pannu, N.S., Read, R.J., Rice, L.M., Simonson, T., and Warren, G.L. (1998) Crystallography & NMR system: A new software suite for macromolecular structure determination. *Acta Crystallogr. D Biol. Crystallogr.* **54**, 905–921
24. Funahashi, J., Takano, K., Yamagata, Y., and Yutani, K. (1999) Contribution of amino acid substitutions at two different interior positions to the conformational stability of human lysozyme. *Protein Eng.* **12**, 841–850
25. Connolly, M.L. (1993) The molecular surface package. *J. Mol. Graphics.* **11**, 139–141
26. Smith, D.K. (2003) Improved amino acid flexibility parameters. *Protein Sci.* **12**, 1060–1072
27. Sugisaki, Y., Ogasahara, K., Miles, E.W., and Yutani, K. (1990) Scanning calorimetric study of tryptophan synthase α-subunits from *Escherichia coli*, *Salmonella typhimurium*, and an interspecies hybrid. *Thermochimica Acta* **163**, 117–122
28. Kaushik, J.K., Ogasahara, K., and Yutani, K. (2002) The unusually slow relaxation kinetics of the folding-unfolding of pyrrolidone carboxyl peptidase from a hyperthermophile, *Pyrococcus furiosus*. *J. Mol. Biol.* **316**, 991–1003
29. Yutani, K., Ogasahara, K., Tsujita, T., Kanemoto, K., Matsumoto, M., Tanaka, S., Miyashita, T., Matsushiro, A., Sugino, Y., and Miles, E.W. (1987) Tryptophan synthase alpha subunit glutamic acid 49 is essential for activity: studies with 19 mutants at position 49. *J. Biol. Chem*. **262**, 13429–13433
30. Nagata, S., Hyde, C.C., and Miles, E.W. (1989) The alpha subunit of tryptophan synthase: evidence that aspartic acid 60 is a catalytic residue and that the double alteration of residues 175 and 211 in a second-site revertant restores the proper geometry of the substrate binding site. *J. Biol. Chem.* **264**, 6288–6296
31. Kabsch, W. and Sander, W. (1983) Dictionary of protein secondary structure: pattern recognition of hydrogen-bonded and geometrical features. *Bioplolymers* **22**, 2577–2637
32. Funahashi, J., Takano, K., and Yutani, K. (2001) Are the parameters of various stabilization factors estimated from mutant human lysozymes compatible with other proteins? *Protein Eng.* **14**, 127–134
33. Kauzmann, W. (1959) Some factors in the interpretation of protein denaturation. *Adv. Protein Chem.* **14**, 1–63
34. Takano, K., Yamagata, Y., and Yutani, K. (1998) A general rule for the relationship between hydrophobic effect and conformational stability of a protein: stability and structure of a series of hydrophobic mutants of human lysozyme. *J. Mol. Biol.* **280**, 749–761
35. Makhatadze, G.I. and Privalov, P.L. (1995) Energetics of protein structure. *Adv. Protein. Chem.* **47**, 307–425
36. Hecht, M.H., Sturtevant, J.M., and Sauer, R.T. (1986) Stabilization of lambda repressor against thermal denaturation by site-directed Gly–Ala changes in alpha-helix 3. *Proteins* **1**, 43–46
37. Herning, T., Yutani, K., Inaka, K., Kuroki, R., Matsushima, M., and Kikuchi, M. (1992) Role of proline residues in human lysozyme stability: a scanning calorimetric study combined with X-ray structure analysis of proline mutants. *Biochemistry* **31**, 7077–7085
38. Nicholson, H., Tronrud, D.E., Becktel, W.J., and Matthews, B.W. (1992) Analysis of the effectiveness of proline substitutions and glycine replacements in increasing the stability of phage T4 lysozyme. *Biopolymers* **32**, 1431–1441
39. Matsumura, M., Becktel, W.J., Levitt, M., and Matthews, B.W. (1989) Stabilization of phage T4 lysozyme by engineered disulfide bonds. *Proc. Natl. Acad. Sci. U.S.A.* **86**, 6562–6566
40. Starich, M.R., Sandman, K., Reeve, J.N., and Summers, M.F. (1996) NMR structure of HMfB from the hyperthermophile, *Methanothermus fervidus*, confirms that this archaeal protein is a histone. *J. Mol. Biol.* **255**, 187–203
41. Usher, K.C., de la Cruz, A.F., Dahlquist, F.W., Swanson, R.V., Simon, M.I., and Remington, S.J. (1998) Crystal structures of CheY from *Thermotoga maritima* do not support conventional explanations for the structural basis of enhanced thermostability. *Protein Sci.* **7**, 403–412
42. Oobatake, M. and Ooi, T. (1993) Hydration and heat stability effects on protein unfolding. *Prog. Biophys. Mol. Biol.* **59**, 237–284
43. Robic, S., Guzman-Casado, M., Sanchez-Ruiz, J.M., and Marqusee, S. (2003) Role of residual structure in the unfolded state of a thermophilic protein. *Proc. Natl. Acad. Sci. USA* **100**, 11345–11349
44. Ota, M., Kanaya, S., and Nishikawa, K. (1995) Desk-top analysis of the structural stability of various point mutations introduced into ribonuclease H. *J. Mol. Biol.* **248**, 733–738
45. Takano, K., Ota, M., Ogasahara, K., Yamagata, Y., Nishikawa, K., and Yutani K. (1999) Experimental verification of the 'stability profile of mutant protein' (SPMP) data using mutant human lysozymes. *Protein Eng.* **12**, 663–672
46. Kraulis, P.J. (1991) MOLSCRIPT: a program to produce both detailed and schematic plots of protein structures. *J. Appl. Cryst.* **24**, 946–950
47. Bacon, D.J. and Anderson, W.F. (1988) A fast algorithm for rendering space-filling molecule pictures. *J. Mol. Graphics* **6**, 219–220